Current Nanomedicine, 2022, *12*, 63-75

RESEARCH ARTICLE

Ultrasmall Superparamagnetic Iron Oxide Nanoparticles Synthesized by Micellar Approach as a Potential Dual-Mode T_1-T_2 Contrast Agent

Watson Beck Jr.[1,2], Laudemir C. Varanda[1,*], Simone J.S. Lopes[1], Daniel A. Moraes[1], Natalia M. Santos[1] and Maria Eduarda S. D. Lino[1]

[1]*Department of Physical Chemistry, Instituto de Química de São Carlos, Universidade de São Paulo, 13566-590, São Carlos - SP, Brazil;* [2]*Instituto Federal de Santa Catarina, IFSC, Campus de Gaspar, Rua Adriano Kormann, 510, Bela Vista, 89110-971, Gaspar, SC, Brazil*

ARTICLE HISTORY

Received: February 22, 2022
Revised: March 16, 2022
Accepted: March 21, 2022

DOI:
10.2174/2468187312666220509213555

Abstract: ***Objective*:** A micellar approach is used to synthesize Ultrasmall Superparamagnetic Iron Oxide Nanoparticles (USPIONs) with an average diameter of 3.4±0.5 nm, suitable for dual-mode T_1-T_2 contrast agents.

Methods: Micelles with 3.8 nm, measured by dynamic light scattering, were obtained by self-organizing the surfactant iron(III) dodecyl sulfate (IDS) in 1-octanol. IDS was prepared by replacing Na^+ cation in sodium dodecyl sulfate molecule, and its critical micelle concentration (CMC) was measured by electrical conductivity. The USPIONs were synthesized in a biphasic system: IDS in octanol (55% above the CMC) and water containing $NaBH_4$.

Results: A yellow precipitate is immediately formed at the water/alcohol interface, rapidly changes to a black one, and transfers to the aqueous phase. The magnetite phase was confirmed by X-ray diffraction and Mössbauer spectroscopy. The magnetic behavior shows a major paramagnetic character with a weak ferromagnetic component at 5 K, the latter attributed to the interparticle couplings below its blocking temperature (T_B = 35 K). The particles were coated with carboxymethyl dextran, showing an isoelectric point of 2.7 with electrokinetic potential around -30 mV in the physiological pH range. Magnetic relaxation measurements showed relaxivity values r_1 = 0.17 mM^{-1} s^{-1} and r_2 = 1.73 mM^{-1} s^{-1} (r_2/r_1 = 10) in a 3T field. These values infer that the ultrasmall size affects the interactions with the protons of the nearby water molecules. The r_2 value decreases because the core magnetization decreases with size; r_1 intensifies due to the high surface.

Conclusion: The results show a system with high colloidal stability, non-cytotoxic, and potential application as T_1-T_2 dual-mode contrast agents.

Keywords: Micellar system, iron(III) dodecyl sulfate, cation-substituted surfactant, USPIONs, biocompatibility, colloidal stability, dual-mode contrast agents.

1. INTRODUCTION

The application of nanoparticles in several technological and biomedical areas is already a reality nowadays. New and potential applications have experienced expressive growth in the scientific literature, mainly due to new, versatile, and improved synthesis routes where greater sustainability and lower production costs are sought [1-4]. Unique and exciting properties have been reported for systems that control at least one or all the parameters such as size, shape, chemical composition, and structure in the nanomaterials synthesis [5, 6].

In the biomedicine field, the advances achieved with multifunctional or theranostic systems in diagnostic imaging, targeting drug carriers, and treatments for diseases such as cancer are noteworthy. Among different nanomaterials, iron oxide nanoparticles with sizes of 3-50 nm and tailored surface chemistry have been experimentally used in numerous biomedical applications [7-13]. Due to their magnetic properties and appropriated surface functionalization, such nanoparticles allow the development of non-invasive diagnostics and therapies [14-16]. Iron oxide presents low toxicity compared to other magnetic materials, for example, transition metal nanoparticles or rare-earth-based compounds. In addition, the biocompatibility of iron oxide nanoparticles has been enhanced by anchoring biocompatible molecules, such as polymers, polysaccharides, fatty acids, and phospholipids, onto the surface of the nanoparticles.

*Address correspondence to this author at the Department of Physical Chemistry, Instituto de Química de São Carlos, Universidade de São Paulo, 13566-590, São Carlos - SP, Brazil; Tel: +55 16 3373-8653; E-mail: lvaranda@iqsc.usp.br

These coatings tend to improve colloidal nanoparticle stability in physiological conditions and blood circulation time, besides providing, in some cases, targeting specific tissues and cell internalization [9, 17-19].

In the field of diagnostic imaging, specifically nuclear Magnetic Resonance Imaging (MRI), interest in new contrast agents called T_2-weighted (negative or dark signal) [20, 21] and T_1-weighted (positive or bright signal) [22, 23] is growing. More recently, agents with dual properties like magneto-optical [24, 25] or T_1-T_2-weighted [26] on single or multifunctional nanostructured materials, called dual-mode T_1 and T_2 MRI contrast agents, have been receiving significant attention. MRI contrast agents act on the relaxation efficiency of protons from nearby water molecules, improving image contrast. T_1-based contrast agents are usually nanoparticles or coordination complexes containing gadolinium or manganese. The metallic element's unpaired electrons accelerate the proton's longitudinal relaxation, producing a bright signal. T_2 contrast agents are based on superparamagnetic nanoparticles, usually iron oxide, the so-called superparamagnetic iron oxide nanoparticles (SPIONs), which decrease the transverse relaxation time of protons, generating dark images [27]. Radiologists prefer T_1 contrast agents because the dark signal of T_2 ones can be confused mainly with internal bleeding and air in the tissues [28]. However, T_1 contrast agents based on gadolinium and manganese have two important disadvantages: (i) the chelate-complexes have a low molecular weight resulting in short circulation times in the body and rapid elimination, that difficult their application in high-resolution MRI; (ii) the gadolinium and manganese ions (from chelates or nanoparticles) are highly toxic, and it can accumulate in the kidneys and brain, leading to systemic renal fibrosis and central nervous system abnormalities [29-32]. Ultrasmall superparamagnetic iron oxide nanoparticles (USPIONs) with a size smaller than 5 nm have emerged in recent years as excellent candidates to act as dual-mode T_1-T_2 and overcome the limitations imposed as contrast agents in high-resolution MRI [33-35]. Both SPIONs nucleus and surface structure play an important role in the relaxation properties, and their effects can be understood by the inner/outer sphere model approach [36-38]. The inner sphere (core) size decreases, leading to an increase in the longitudinal relaxivity (r_1), *i.e.*, the specific surface increases as the size decreases, favoring interactions with water protons. Furthermore, according to the external sphere model, reducing the size decreases the magnetization and, consequently, the transverse relaxivity (r_2) due to ordered spins volume decreases [39, 40]. As a result, USPIONs present a T_1-weighted signal because they increase the r_1 value and decrease both r_2 and the r_2/r_1 ratio [38].

According to the methodology, SPIONs with different levels of control over size, shape, size distribution, crystalline structure, and chemical composition can be obtained. However, SPIONs for biomedical applications require high uniformity of the mentioned features, and not all reported methods have this characteristic [41]. Thermal decomposition has been highlighted in the literature because it offers fine control over the SPION size and morphology [6, 28] and is preferred for USPION synthesis [38]. However, there is the disadvantage that the resulting nanoparticles are hydrophobic (non-water dispersible) due to the presence of organic molecules that remains bound onto the nanoparticle surface, requiring additional functionalization for biomedical application [23]. Traditional coprecipitation methods in the aqueous medium have evolved in controlling nanoparticles' size and shape but still present a challenge in synthesizing ultrasmall nanoparticles [13, 42].

Here we describe a simple micellar approach to the synthesis of water-dispersible USPIONs (magnetite) using iron(III) dodecyl sulfate (IDS) as a cation-substituted surfactant in a biphase octanol-water medium. The USIONs present an average particle size diameter of 3.4 nm with narrow size distribution and electrokinetic potential (zeta) around -30 mV after carboxymethyl dextran (a biocompatible polysaccharide, CMDex) coating. The partial paramagnetic behavior of the USPIONs and CMDex-coated USPIONs concerning their magnetic-relaxation properties (T_1 and T_2) and the effects of cytotoxicity in cancerous and noncancerous cells were also evaluated. The CMDex-coated USPIONs present all desirable characteristics for application as dual-mode T_1-T_2-weighted MRI contrast agent: expressive colloidal stability, compatible biomedical required size, partial paramagnetic and ferromagnetic behavior, adequate low relaxivity ratios (r_2/r_1 ~10), and negligible cytotoxicity.

2. MATERIALS AND METHODS

2.1. Materials

Iron(III) nitrate nonahydrate ($Fe(NO_3)_3.9{\cdot}H_2O$, 98%), sodium borohydride ($NaBH_4$, 98%), and carboxymethyldextran sodium salt (CMDex, ~10-20 KDa) were purchased from Aldrich. Sodium dodecyl sulfate (SDS, 95%), nitric acid (HNO_3, 69-70%), and 1-octanol ($C_8H_{17}OH$, 99%) were purchased from JT Baker. All reagents were used as received, and the experiments were performed using ultrapure water (18 MΩ cm^{-1}).

2.2. Synthesis of Iron(III) Dodecyl Sulfate (IDS) Surfactant

IDS was prepared by mixing equal volumes of equimolar SDS and $Fe(NO_3)_3.9\ H_2O$ (0.1 mol L^{-1}) aqueous solutions under vigorous magnetic stirring at room conditions for 1 hour. After that, the stirring was stopped, and the solution was aged at 4 °C for six hours. Then, the yellow precipitate was washed five times with cold water, separated by filtration, and dried under a vacuum.

2.3. Synthesis of USPIONs

A solution of 1.38 mmol L^{-1} (~1 g, around 55% above the measured CMC) of IDS in 1-octanol (250.0 mL) was added to water (100 mL), leading to a biphasic system where the water is the bottom phase. Under low magnetic stirring and a blank of N_2, $NaBH_4$ (130 mmol, 0.05 g) was added to the system. An immediate effervescence is observed at the water/alcohol interface, resulting in an orange

residue. The residue was readily transferred to the aqueous phase as soon as it formed. It acquires black color a few minutes later and is attracted to the magnetic bar surface. When the gas detachment was stopped, the black precipitate was separated by centrifuging, washed three times with ethanol, and dried under vacuum.

2.4. USPIONs Surface Modification with CMDex

As-synthesized USPIONs (50 mg) were dispersed in water (10.0 mL), and the pH was adjusted to 11 with 0.1 mol L^{-1} NaOH aqueous solution. The temperature was increased up to 45 °C under stirring, and 5.0 g L^{-1} of CMDex aqueous solution (10.0 mL) was added to the system. After 1 hour, the system was cooled to room temperature, and the suspension was dialyzed overnight in water using a 12000-14000 nominal molecular weight cutoff membrane. Then, the black powder was separated by centrifugation and dried under a vacuum.

2.5. Relaxation Measurements

Relaxation measurements were performed on a clinical 3.0 T MRI scanner (Achieva, Philips, Best, The Netherlands) using a 32-channel head coil. Physiological saline solution (Simulated Body Fluid, SBF [43]) of CMDex-coated SPIONs at a concentration range of 0 (pure water) to $2.0x10^{-3}$ mol L^{-1} of Fe was employed. Atomic absorption analyses previously determined the iron concentration. For T_1 measurements, the 2D spin-echo sequence was used with the following parameters: *TE* = 15.5 ms, *TRs* = 0.12, 0.14, 0.16, 0.18, 0.20, 0.30, 0.40, 0.50, 0.60, 0.70, 0.80, 0.90, 1.00, 1.20, 1.40, 1.60, 1.80, 2.00, 2.50, 3.00, and 3.50s. For T_2 measurements, the 2D conventional CPMG (Carr Purcell Meiboom Gill) sequence was used with the following parameters: *TR* = 5 s; *TEs* = 20, 40, 60, 80, 100, 120, 140, and 160 ms. The voxel size was kept constant for both measurements in 0.49x0.49x4.00 mm. The R_1 and R_2 values were calculated by fitting the averaged pixel intensity to $I = I_0\left(1 - exp(-R_1 \times TR)\right)$ and $I = I_0 exp(-R_2 \times TR)$, respectively. The relaxivity values ($r_{1,2}$) were calculated from the relaxation ratios ($R_{1,2}$) according to the general relation: $R_{1,2} = 1/T'_{1,2} + r_{1,2}C$ corresponding to the linear fit on the experimental *1/T versus* [Fe] curves. $T'_{1,2}$ is the relaxation time in pure media where *C* indicates nanoparticle concentration.

2.6. Cell Culture and Cytotoxicity Assay

Four cell lines were used to evaluate USPIONs cytotoxicity: the human lung adenocarcinoma cell line A549 (ATCC® CCL-185), the cancerous cells HeLa (human cervical carcinoma), noncancerous cells NCTC L929 (connective tissue fibroblasts from mice), and the human lung non-tumor cell line MRC-5 (ATCC® CCL-171). Cells were cultured in DMEM (Dulbecco Modified Eagle Medium) supplemented with 10% fetal bovine serum and penicillin (100 units mL^{-1}), gentamicin (50 mg L^{-1}), and amphotericin (25 µg mL^{-1}). A standard number of cells were cultivated ($1.0x10^6$ cells) in 75 cm^2 flasks (Corning) and maintained at 310 K, under a humidity atmosphere and 5% CO_2 in the air, changing the culture medium every two days. The development of the cellular growth and the morphology of each culture was followed by using an inverted phase-contrast microscope to assess the degree of confluence and confirm the absence of contaminants. Then, cells were detached from culture flasks by trypsinization with saline-trypsin-solution, centrifuged (1200 rpm for 5 minutes at 4 °C), and resuspended in a culture medium. Hence, cells are counted in a Neubauer chamber by the Trypan Blue dye exclusion method. The concentration was adjusted for $1.5x10^4$ per well to proceed with the cell viability experiment. Cell viability was evaluated by the MTT assay (3-(4,5-dimethylthiazol-2-yl)-2,5-diphenyltetrazolium), which is well-established cell viability colorimetric assay [44]. Viable cells can reduce the tetrazolium ring into an insoluble purple formazan crystal, which can then be dissolved in an organic solvent and quantified by measuring the solution's absorbance at 540 nm. The amount of absorbance measured is directly proportional to the number of living cells. For the viability experiments, cultured cells were used between the fourth and seventh passage to avoid alterations in the cellular morphology. Samples of 150 µL of the cell lines ($1.5x10^4$ cell mL^{-1}) in the culture medium were added to each well of a 96-well tissue culture plate. Then, they are incubated at 310 K for 24 h in an atmosphere of 5% CO_2 to allow the cells to adhere. Subsequently, aliquots of 0.75 µL of water-dispersed SPIONs were added in different concentrations (14.0, 7.0, 3,5, and 1.7 µg mL^{-1}) in each well. Then, 0.75 µL distilled water was added to 9 wells for the cell viability control, and the plates were incubated again for 48 h. Next, 50 µL of MTT (1 mg mL^{-1}) was added to each well, and the cells were incubated for 3 h. Thus, MTT solutions were carefully removed by a multichannel micropipette, and the formazan crystals were solubilized with 150 µL of isopropyl alcohol. The plates were incubated for 20 minutes in the same conditions for better solubilization. Finally, the absorbance was measured in a microplate spectrophotometer reader (BioTek™, Epoch™) at a wavelength of 540 nm. The relative cell viability (%) was calculated according to the relationship $(ATC/AC)x100$, where *ATC* is the absorbance of the treated cell solution with USPIONs in different concentrations and *AC* is the absorbance of the control cells without nanoparticles. The experiment was performed in triplicate. The data obtained were treated using GraphPad Prism 5.01, and differences were considered statistically significant when $p > 0.05$.

2.7. Characterization

Thermogravimetric analysis (TGA-DTA) was performed in a Shimadzu TA-50WSI attached to a TGA50 module. The sample weighing about 5 mg was analyzed under a synthetic airflow of 100 mL min^{-1} with a heating rate of 10 °C min^{-1}. Elemental analysis (EA) was carried out using a Perkin Elmer CNH 2400 elemental analyzer for the elements C, N, H, and S resulting in Anal. Calcd for IDS surfactant: C, 40.0; H, 8.1; N, 2.0; S, 8.9. Found: C, 41.9; H, 8.2; N, 2.6; S, 8.0. Fourier-Transform Infrared Spectroscopy (FTIR)

spectra were recorded in a Shimadzu IRPrestige-21 in the range from 4000 to 400 cm^{-1} at a resolution of 4 cm^{-1} using the KBr pellets. Energy-Dispersive X-ray Spectroscopy (EDS) was performed in an EDS. Link Analytical (Isis System Series 200) with a SiLi Pentafet detector and ultrathin ATW II window coupled to a Zeiss-Leica/440 scanning electron microscopy. The Critical Micelle Concentration (CMC) of IDS in 1-octanol was simultaneously determined by electric conductivity measurements and the Dynamic Light Scattering (DLS) technique. The electric conductivities of nine octanolic IDS solutions with different concentrations were measured in triplicate using a CRISON GLP32 conductivity meter. The average values were plotted *versus* concentration, and the CMC was obtained by the intercept of the different curve slopes. These nine IDS solutions were also analyzed using a Zetasizer Nano ZS from Malvern Instruments to determine the micelle's formation and its hydrodynamic size. Transmission Electron Microscopy (TEM) of the USPIONs was performed using a JEOL JEM2100 microscope operating at 200 kV. The samples were prepared by dropping ethanolic dilute particle suspensions onto a carbon-coated copper grid, and the solvent was evaporated at room temperature. The size distribution, average particle size (D_{TEM}), and Standard Deviation (SD) were determined by measuring at least 200 nanoparticles using the free software ImageJ v1.53c. X-ray powder diffraction analysis (XRD) was performed in a Rigaku RINT2000 diffractometer using Cu Kα radiation (λ = 1.5406 Å) in the range of 25-70° in 2θ with a step of 0.02° and 3 seconds/step. Mössbauer spectrum was obtained by using a conventional apparatus of ^{57}Co source in Rh matrix at 4.2 K using the method of constant acceleration. The spectrometer velocity was calibrated using a pure iron foil. Electrophoretic mobility measurements were performed in a 10^{-3} mol L^{-1} KNO_3 background aqueous electrolyte solution in a Zetasizer Nano ZS from Malvern Instruments using diluted as-synthesized as CMDex-coated USPIONs suspensions at different pH values adjusted with diluted HNO_3 and NaOH aqueous solutions. Magnetic studies were carried out by using a commercial SQUID. A magnetic hysteresis loop was obtained with fields up to 80 kOe at 5 K. The temperature dependence of magnetization was evaluated in both Zero-Field-Cooling (ZFC) and Field-Cooling (FC) modes with the maximum applied field of 50 Oe and temperature ranging between 5 and 300 K.

3. RESULTS AND DISCUSSION

3.1. Iron(III) Dodecyl Sulfate Synthesis

Using a cation-substitute surfactant in nanoparticle synthesis intends to eliminate effects related to the presence of solvated counterions in the micelles. The interactions between surfactant head and counterions charges often affect physicochemical properties of both micelle and reverse micelle [45-47], like its size, micellar structure stability, and the elasticity of their walls. Such interactions could also influence the system stability and, consequently, the nanoparticle features [48]. In this work, we used a simple cation exchange in aqueous media at low-temperature aging, resulting in a more stable compound. This procedure has also been successfully applied to Fe^{2+}, Co^{2+}, Ni^{2+} and Cr^{3+} cations (data not shown). Since IDS complex was not yet reported as an isolated compound in the literature, except as an in-situ generated intermediate for some catalytic reactions [49, 50], its molecular structure was investigated. The success of cation substitution was firstly proved by EDS analysis. The EDS spectrum of IDS (Fig. **S1a**) presents only the presence of L_α, K_α, and K_β characteristic lines of iron element at 0.71, 6.40, and 7.05 keV, respectively, besides the lines at 0.28, 0.53, and 2.31 keV corresponding to typical emission energy from K_α lines of C, O, and S, respectively. No characteristic sodium line was observed at around 1.0 keV.

TGA-DTA, EA, and FTIR analyses corroborate the IDS formation and indicate the molecular structure $[Fe(DS)_2(H_2O)_4NO_3]$ for IDS cation-substituted surfactant with a molecular weight of 720.7 g/mol (DS represents dodecyl sulfate ligands). The TGA-DTA curves in Fig. (**S1b**) show a first mass loss between 25 and 105 °C attributed to the dehydration process of four water molecules (Calcd. = 10.0%, Measured = 10.2%). One can also observe a mass loss in two steps (28.2 and 26.1%) in the temperature ranges 105-150 °C and 150-215 °C, respectively, corresponding to the oxidation of the dodecyl tail of the two molecules' ligands. The complex presents an additional mass loss up to 405 °C, which was assigned to the loss of one nitrate ion (Calcd. = 8.6%, Measured = 8.7%). The final thermal event at the temperature range of 510-645 °C corresponding to the sulfate group mass loss (Calcd. = 15.5%, Measured = 15.6%) resulted in an 11.2% residual product assigned to the hematite (α-Fe_2O_3) formation as shown by the XRD analysis (Fig. **S1c**). The hematite residue stoichiometry allows the calculation of the iron amount from TGA-DTA analysis is 7.7%, which is very close to the theoretical value calculated for $[Fe(DS)_2(H_2O)_4NO_3]$ complex (7.9%). This molecular structure is corroborated by CHNS elemental analysis (see Experimental section).

FTIR analysis also infers the molecular structure of IDS formation (Fig. **S1d**). Although FTIR spectra of SDS and IDS show remarkable similarity, some differences are noticeable. Absorption bands in 3400 and 1650 cm^{-1} appear broader and more intense in the IDS spectrum, respectively ascribed to OH stretching and HOH bending to four water molecules into IDS molecular structure [51]. The sulfate headgroup can be present in IDS structure as a free counterion or coordinated to iron(III) cation as a unidentate, bidentate, or bridging bidentate ligand [51]. Each coordination form presents different infrared absorptions, and the main differences are expected in the interval 1350-750 cm^{-1} [52]. The SDS spectrum shows characteristic absorption bands of asymmetric and symmetric stretching modes of the sulfate group in a C_{3V} symmetry with bands at 1251 and 1220 cm^{-1} $(\nu_{as,O-S-O})$ and 1083 cm^{-1} $(\nu_{s,O-S-O})$ respectively. Although these three bands are also observed for IDS, the latter two bands are shifted to lower wavenumber, 1209 and 1068 cm^{-1}, respectively. These downshifts are associated with strong electrostatic effects involving coordination of sulfate

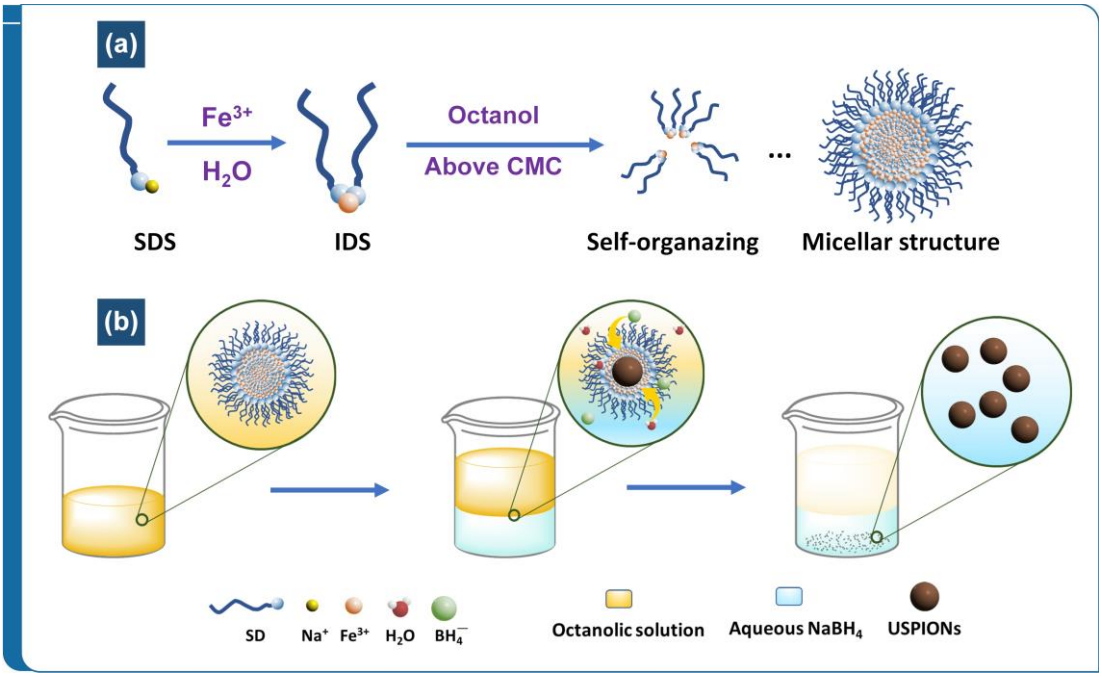

Scheme 1. Schematic representation of the USPIONs synthesis route. (**a**) Na^+ cation substitution from sodium dodecyl sulfate (SDS) to obtain the Fe(III) dodecyl sulfate (IDS). The IDS molecules are self-organized in the octanol in a concentration slightly above its critical micelle concentration (CMC), resulting in a micellar colloidal dispersion. (**b**) Micellar dispersion was mixed with an aqueous $NaBH_4$ solution leading to a biphasic system. Water molecules and BH_4^- ions (reducing agent) percolate into de micelle at the biphasic interface region reducing the Fe cations to produce the USPIONs. The fresh nanoparticles precipitate into the water phase. (*A higher resolution / colour version of this figure is available in the electronic copy of the article*).

headgroup and the trivalent iron cation. Similar observations have been reported for trivalent Pr and Fe complexation with dodecyl sulfate ligands [53, 54]. The two ($\nu_{as,O-S-O}$) bands appear enlarged in the direction of lower wavenumber. Since some absorption bands between 1150 and 1190 cm^{-1} are attributed to hydrogen bonding interactions between coordinated water molecules and sulfate headgroups of coordinated dodecyl sulfate [52], this enlargement of ($\nu_{as,O-S-O}$) bands evidence the four water molecules probably completing the first coordination sphere of iron(III) cation. The NO_3^- anion can coordinate to *d*-metal cation as a unidentate, chelating bidentate, or bridged bidentate. In these cases, the symmetry of the coordinated anion is C_{2v} and should be observed the set of bands associated with the split of ν_3 mode, generally at regions 1530-1480 and 1290-1250 cm^{-1}, 1565-1500 and 1300-1260 cm^{-1} and, 1650-1600 and 1225-1170 cm^{-1}, respectively for the three kinds of coordination [55, 56].

As shown in Fig. (**S1d**) and its inset, the region between 1800-800 cm^{-1} of IDS is complex by containing several bands related to the alkyl chain and SO_4^{2-} ion, making it impossible to attribute certainty to the nitrate ion type of coordination.

3.2. Micelle System Formation from IDS Complex

The CMC of IDS in 1-octanol was studied by measuring two properties of octanolic IDS solutions: electrical conductivity and Dynamic Light Scattering (DLS). Such properties were chosen based on the behavior of surfactant solutions. At low concentrations, surfactant molecules are randomly spread through the solution. When the system reaches a specific surfactant concentration, the molecules organize themselves as micellar aggregates to minimize surface energy. Such structural modification affects system properties, including surface tension, osmotic pressure, turbidity, electrical conductivity, and light scattering. It is important to note that, depending on the characteristics of the solvent, direct or reverse micellar aggregates can be reached, *i.e.*, the molecules can be organized with their polar head outside or inside the micellar aggregate, respectively. The reverse micellar system is generally observed when a weakly polar solvent is employed, which justifies our choice of 1-octanol as the solvent. The different steps of the USPIONs synthesis from the preparation of cation-substituted surfactant (IDS) are shown in Scheme **1**. After the IDS purification, its molecules self-organize to form the micellar system in octanol. This colloidal dispersion is mixed with the aqueous solution containing the reducing agent ($NaBH_4$). The percolation of water molecules and BH_4^- ions into the micelle occur at the water/octanol interface, leading to the USPIONs formation, followed by its separation towards the aqueous phase.

As shown in Fig. (**1**), the electrical conductivity increases linearly with the IDS concentration, but an abrupt discontinuity can be observed at 0.90 mmol L^{-1}. Such behavior is explained by a decrease in transport number, which occurs due to the agglomeration of dodecyl sulfate monomers to form micellar aggregates. The solid lines fitted to the two linear behaviors intercepts at 0.90 mmol L^{-1}, which corresponds to the CMC of IDS in 1-octanol. Light scattering

measurements corroborate this value of CMC. The concentration increases near 0.90 mmol L^{-1} resulting in an abrupt increase of hydrodynamic size molecular species dispersed into the medium (individual isolated IDS molecules) from around 0.1 nm to near 4 nm. It implies that from 0.9 mmol L^{-1}, the surfactant molecules in the solvent themselves organize in micellar aggregates whose stable hydrodynamic sizes are around 3.5-4.0 nm.

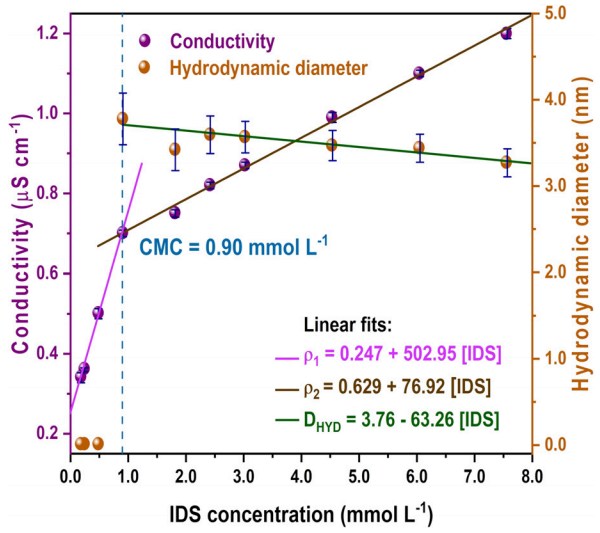

Fig. (1). Measurements of electrical conductivity and hydrodynamic diameter as a function of IDS concentration. Both techniques infer that the IDS CMC in 1-octanol is at 0.90 mmol L^{-1} IDS concentration and the DLS measurements show the reverse micelle aggregates with a hydrodynamic diameter of 3.5 nm. (*A higher resolution / colour version of this figure is available in the electronic copy of the article*).

3.3. Ultrasmall Iron Oxide Nanoparticles (USPIONs) Synthesis

The USPIONs were prepared from an octanolic solution of iron(III) dodecyl sulfate (IDS) with IDS concentration around above 50% of its critical micelle concentration (CMC). The control over particle size and shape is achieved since micellar aggregates act as nanoreactors and steric stabilizers, inhibiting the freshly formed particles' uncontrolled growth and aggregation [57-59]. The cation-substituted surfactant aims to avoid undesirable counterions inside the micelles, which could interact with the surfactant polar head and destabilize the micellar structure during the nanoparticle synthesis. Furthermore, the proposed method allows the particle formation to occur with high homogeneity because there is no dependency on the coalescence between two different micelles structures, as in a microemulsion system, carrying the cation and de reducing agent separately. Thus, the magnetic nanoparticles were obtained using a biphasic system composed of water (bottom phase) and a 1.38 mmol L^{-1} IDS octanolic solution (top phase). After the solubilization of $NaBH_4$ in the aqueous phase, BH_4^- ions and some water molecules percolate into the micelle's aggregates located near the mixture interface. The presence of reducing ions and water molecules in the micelles promotes the reduction of iron(III) ions and starts nucleation and growth processes for particle formation. At this point, the micellar stability was not enough to maintain the freshly nucleated particle suspended in the alcoholic phase. The nanoparticles were systematically transferred from the interface region to the aqueous phase.

According to TEM, XRD, and Mössbauer spectroscopy analyses, ultrasound magnetite nanoparticles were obtained. Typical TEM images of the as-synthesized magnetite nanoparticles (Fig. **2a** and **2b**) reveal that the proposed synthetic route results in monodisperse-like spherical nanoparticles. The log-normal distribution fitted on the experimental size diameter (Fig. **2c**) reveals an average diameter of 3.4 ± 0.5 nm, which corresponds to a polydisperse degree (σ) of 15%, only 5% above the limit considered for a monodisperse system (10%). The XRD pattern in Fig. (**2d**) shows peaks centered at 30.0, 35.3, 42.9, 53.4, 56.9, and 62.6° in 2θ, which are attributed respectively to (220), (311), (400), (422), (511), and (440) planes of spinel structure of magnetite phase, according to the standard XRD pattern JCPDS number 19-629. Since the magnetite and maghemite phases are isostructural (lattice constants parameter 8.396 and 8.351 Å, respectively), both are magnetic and have a black or dark brown color on the nanometer scale making their differentiation by X-ray diffractometry is difficult. However, magnetite presents both Fe(II) and Fe(III) ions distributed in the octahedral and tetrahedral sites, whereas maghemite has only Fe(III) ions in its composition [13, 60]. Mössbauer spectroscopy gives information about the valence of the iron ions, and it can be used to distinguish magnetite and maghemite phases. The Mössbauer spectrum shown in Fig. (**2e**), as expected for a typical magnetite behavior, corresponds to two sextets attributed respectively to Fe(III) ions in tetrahedral sites (site A) and Fe(II) and Fe(III) ions in octahedral sites (site B).

The presence of Fe^{3+} and Fe^{2+} in the octahedral sites can be approximated to the $Fe^{2.5+}$ valence because the electron dislocation allows the nucleus to sense an average valence [60]. The main Mössbauer parameter (Table **1**) agrees with the expected for the magnetite phase. The observed hyperfine fields of H_{hyp} = 50.2 T and H_{hyp} = 46.9 T for sites A and B, respectively, are smaller than expected values for magnetite measured at 4.2 K, which is a result of the ultrasmall dimensions of the particles, probably caused by the spin-canting effects from the atoms on nanoparticles surface [60, 61].

The room temperature hysteresis loop (Fig. **3a**) of USPIONs is the typically expected profile for a paramagnetic material. The magnetization increases slightly and steadily with increasing applied magnetic field, almost parallel to the x-axis. Such behavior was already expected for ultrasmall magnetic particles [28], and to obtain more information about the system, measurements were performed at a temperature of 4.2 K (Fig. **3a**). At this temperature, with the magnetic moments remaining blocked, it is possible to observe a superposition of the paramagnetic behavior of the system (the region where the magnetization increases linearly with the applied field) with a subtle ferromagnetic coupling. This last behavior is observed in the low field region

Table 1. Mössbauer parameters at 4.2 K from the as-synthesized USPIONs.

Site	Mössbauer Parameter*				Assignment
	δ (mm s^{-1})	Δ (mm s^{-1})	B_{hyp} (T)	Γ (%)	
A	0.28	0.00	50.2	35.1	Fe^{3+}_{Tet}
B	0.41	-0.04	46.9	64.9	$Fe^{2.5+}_{Oct}$

* Isomer shift (δ, mm s^{-1}), quadrupolar splitting (Δ, mm s^{-1}), hyperfine field (B_{hyp}, T), and relative area (Γ, %).

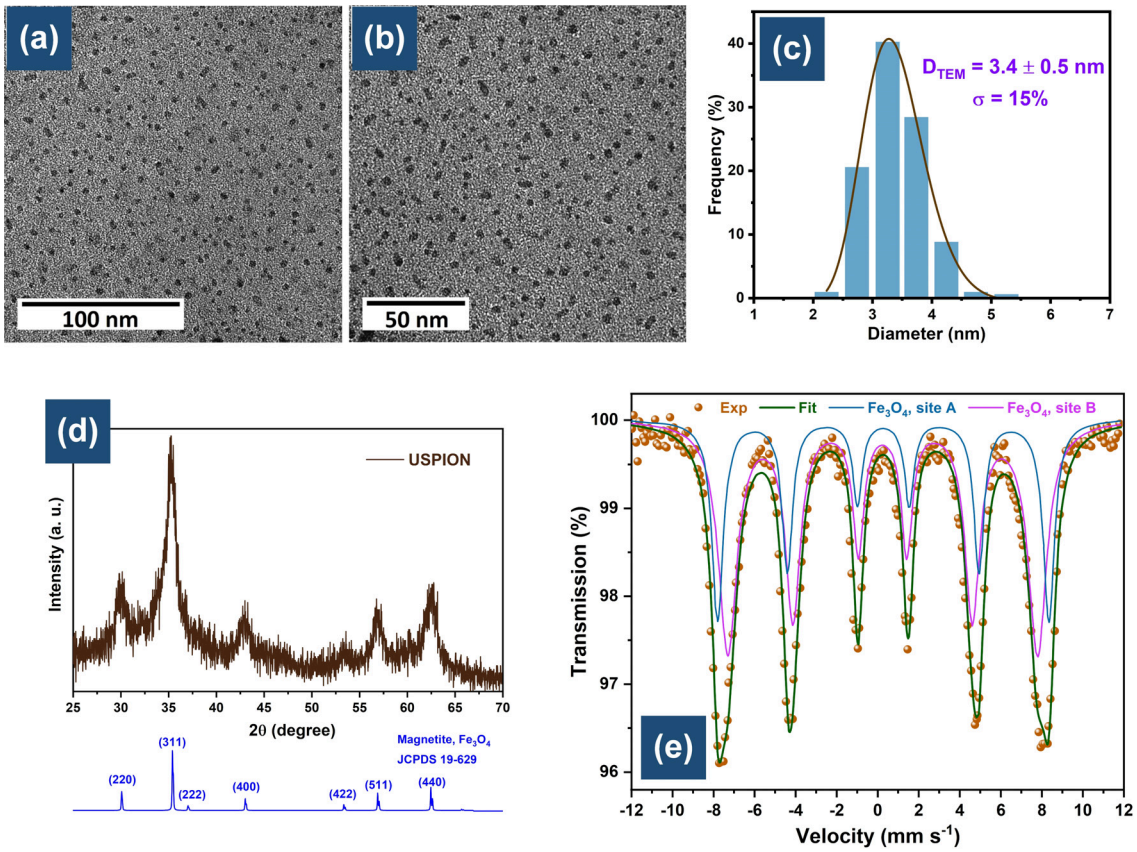

Fig. (2). As-synthetized USPIONs (**a**, **b**) TEM images at different magnifications, (**c**) Size distribution with a log-normal fit, (**d**) XRD patterns with the magnetite standard pattern (JCPDS 19-629), and (**e**) Mössbauer spectrum at a temperature of 4.2 K. (*A higher resolution / colour version of this figure is available in the electronic copy of the article*).

and is characterized by a rapid increase in magnetization with the applied field and has been attributed to interparticle interactions or couplings [62]. Because of their small size, the USPIONs are single magnetic domains, and the behavior is correlated to the interactions between these single domains that remain blocked at low temperatures. In the inset in Fig. (**3a**), it is possible to observe this region, which shows low coercivity (~300 Oe) and remanence (~0.5 emu g^{-1}), even at 5 K. As also shown in the inset in Fig. (**3a**), the material does not show magnetic saturation even in fields up to 80 kOe, precisely because of its primarily paramagnetic behavior. These results are consistent with the temperature dependence of magnetization shown in FC/ZFC curves (Fig. **3b**). The peak in the FC curve (and the change in behavior of the ZFC ones) corresponds to the superparamagnetic blocking temperature (T_B) of the sample (T_B = 35 K), which is lower than values 107 and 45 K reported respectively for magnetite nanoparticles with 11.5 and 4 nm [63]. The low T_B results from the ultrasmall dimensions of analyzed particles. As SPIONs remain with their magnetic moments blocked below T_B, the single domain interparticle coupling leads to the emergence of the ferromagnetic behavior observed in the hysteresis loop. Another indication of this interaction is the spacing between FC and ZFC curves over a long temperature range, although other effects contribute to this behavior [64]. It is noteworthy that for applied fields higher than 10 kOe and lower than -10 kOe, the magnetization curve presents a linear behavior with no saturation typically observed in paramagnetic materials. Such materials are promising T_1 contrast agents since they enhance the T_1 effect by their large surface area with five unpaired electrons and suppress the T_2 effect by their small magnetic moment [28, 30, 65].

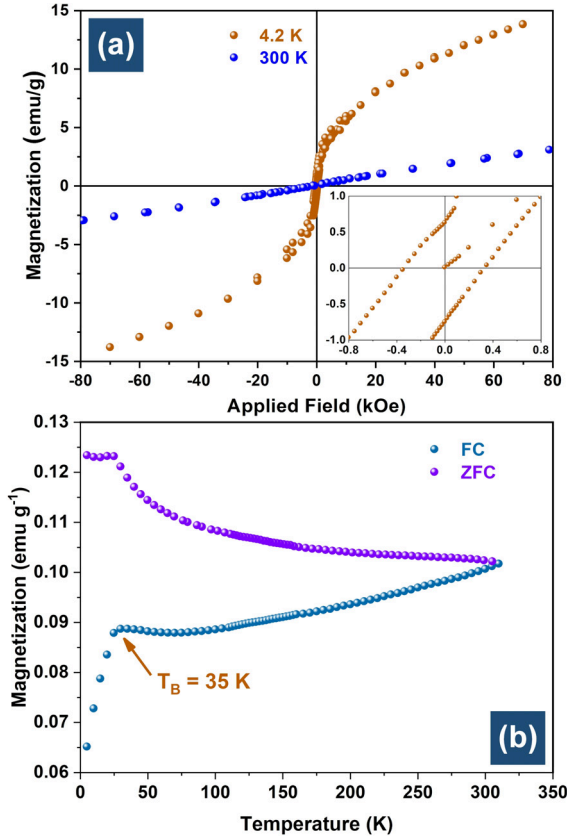

Fig. (3). (**a**) Magnetic hysteresis loop of as-synthesized magnetite nanoparticles measured at 4.2 K and 300 K. The inset corresponds to the enlargement of the low applied field region of the 4.2 K curve; (**b**) Field-cooled (FC) and zero-field-cooled (ZFC) magnetization curves as a function of temperature measured at the maximum applied field ($H_{FC,\,max}$) of 50 Oe. (*A higher resolution / colour version of this figure is available in the electronic copy of the article*).

3.4. CMDex Coating

FTIR spectra of uncoated USPIONs, pure CMDex, and CMDex-coated USPIONs are presented in Fig. (**4a**). The USPIONs spectrum shows two bands at 1635 cm^{-1} and the broadband in the region of 3400 cm^{-1} assigned respectively to O-H bending (δ_{O-H}) and stretching (ν_{O-H}) of hydroxyl groups or water molecules adsorbed onto the surface of the nanoparticles. The broadbands in the region of 1150-800 cm^{-1} are assigned to overlapping bands of S-O stretching vibrations ($\nu_{S=O}$ and ν_{S-O}) from some strongly adsorbed sulfate ions onto the nanoparticle surface remains from IDS [13]. The three bands at 694 cm^{-1}, 585 cm^{-1}, and 460 cm^{-1} are attributed to symmetric and asymmetric stretching of the Fe-O bond, typically observed for the magnetite phase [60]. The CMDex spectrum presents weak intensity bands at region 940-730 cm^{-1} assigned to the vibrations of the glycoside bands (glucopyranose) from α-1.6 bonds [66]. The stretching bands corresponding to the C-O vibrations modes are overlapped with other vibrations. However, it can be observed at two different wavenumber regions: 1190-950 cm^{-1} assigned to the ν_{C-O-C} and ν_{C-O} and at 1640-1435 cm^{-1} attributed to symmetric and asymmetric modes of the carboxylic ions, $\nu_{as,s\,C=O}$. The stretching of C-H bonds ($\nu_{C\text{-}H}$), as well as the bending modes ($\delta_{C\text{-}H}$), can be observed at 2990-2820 cm^{-1} and 1430-1300 cm^{-1}, respectively [66, 67]. Besides the bands present at the pure USPIONs spectrum, the CMDex-coated USPIONs ones show the typical bands from CMDex, identified by red arrows in Fig. (**4a**), inferring the success of the surface modification process.

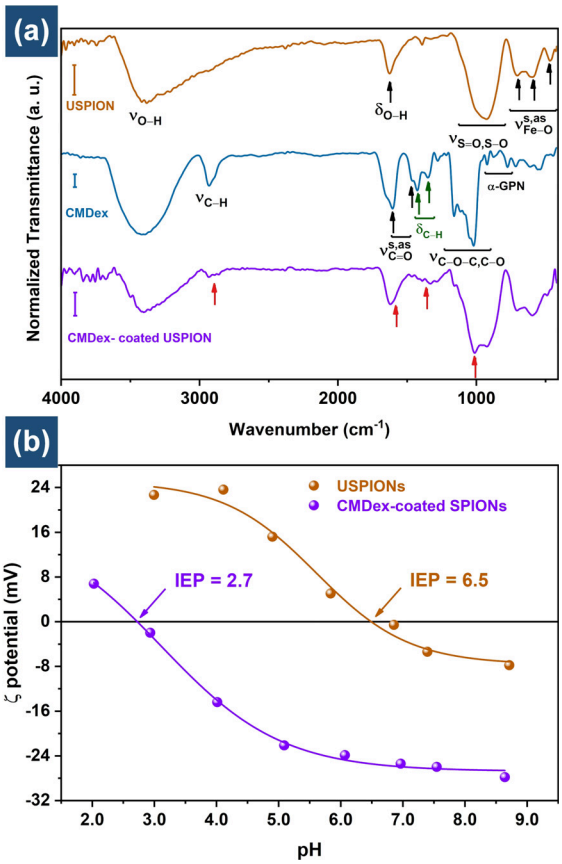

Fig. (4). (**a**) FTIR spectra obtained for as-synthesized USPIONs, pure CMDex, and CMDex-coated USPIONs, and (**b**) the electrophoretic measurement (zeta potential) as a pH function of the uncoated and CMDex-coated USPIONs. (*A higher resolution / colour version of this figure is available in the electronic copy of the article*).

DLS measurements were performed for uncoated and CMDex-coated USPIONs (Fig. **4b**). The isoelectric point (IEP) determines the pH in which molecular species or particle surfaces have no net electrical charge, *i.e.*, the pH at which a colloidal particle remains stationary in an electrical field. It can be used to evaluate the presence of charged species on the nanoparticle's surface and, in this study, to investigate the pH range at which the CMDex-coated nanoparticles show colloidal stability. As presented in Fig. (**4b**), the coating process decreases the IEP from 6.5 to 2.7 of the uncoated and coated USPIONs. This decrease infers the presence of CMDex molecules on the nanoparticle's surface and can be explained by the presence of hexuronic (carboxylic) acid groups remaining on the bonded CMDex chains. The carboxylic acid groups have a pKa value of around 3, which imparts a negative charge over almost the entire pH range. Therefore, CMDex-coated magnetite nanoparticles

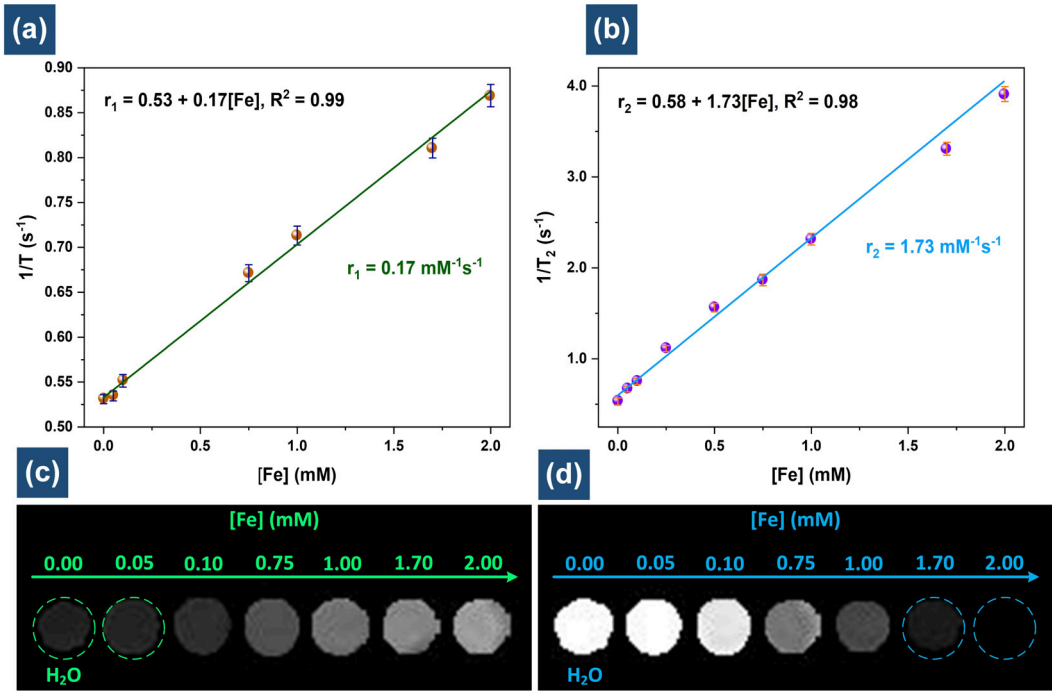

Fig. (5). Plots of (**a**) $1/T_1$ and (**b**) $1/T_2$ as a function of Fe concentration (mM) of SBF aqueous samples suspension of CMDex-coated USPIONs using a 3.0 T MR scanner. The slopes in each plot correspond to r_1 and r_2 values, respectively. (**c**) R1 and (**d**) R2 map images of SBF aqueous USPIONs suspensions as a function of Fe concentrations (mM). (*A higher resolution / colour version of this figure is available in the electronic copy of the article*).

have a negative surface charge in pH above 2.7 and, therefore, present colloidal stability in pH values around physiological conditions (pH values between 6-8), with ζ potential ranges -25 to -30 mV, which is the first requirement for biomedical applications.

3.5. MRI Contrast Agent and Cytotoxicity Assays

The coated USPIONs performance concerning a potential application as a dual-mode T_1-T_2-weighted was evaluated, and the results are shown in Fig. (**5**). The r_1 and r_2 relaxivity values were 0.17 and 1.73 $mM^{-1}s^{-1}$, respectively (Fig. **5a** and **5b**). Although the r_1 value is not that high, similar values have been reported previously for Dextran-PEG-encapsulated iron oxide nanoparticles around 9 nm in size [68]. It is important to note that the r_2 value, in contrast, is also not high as expected for iron oxide nanoparticles, even with a similar core size [38]. Other papers reported similar r_1 and r_2 values for MnO nanoparticles coated with silica [69] or APTS-CMDex [23]. Besides the individual values of the relaxivity, an essential parameter to distinguishing T_1 and T_2 contrast agents is relaxivity ratio values (r_2/r_1), which must be closed to 1 (ideal) and acceptable when the values are ≤ 10 [34, 35, 38]. In this work, our relaxivity ratio can be considered low (r_2/r_1 = 10) and close to the values reported for similar materials as potential dual-mode contrast agents. In the T_1-weighted image (Fig. **5c**), a good bright MRI signal-enhancement effect was obtained at different Fe concentrations, highlighting the iron concentration's signal above 1.7 mM. The same result, but more clearly, occurs for the MRI dark signal (Fig. **5d**) in similar concentrations. Two factors contribute to our results: the ultrasmall size of the particles and the coating with CMDex, which decrease the core magnetization and intensify the surface properties in the interactions with the protons of the water molecules.

Cell viability assays are essential in medicinal or biomedical chemistry since they reveal a toxicant agent's cellular response. They also provide knowledge on cell death, survival, and the proportion of both phenomena. Therefore, the effect on cell viability (cytotoxicity) of USPIONs was evaluated towards four cell lines HeLa (human cervical carcinoma), A549 (lung cancer), MRC-5 (non-tumor lung), and L929 (connective fibroblasts, mice) per MTT assay, and the results are shown in Fig. (**6**). It was observed that CMDex-coated USPIONs did not significantly modify the viability of the cells compared to control (cells without nanoparticles) at the concentrations tested (14 to 1.72 μg mL^{-1}). In all cases, tumoral or non-tumor cells, the cell viability was kept up to 90%, considering the statistical variation and the experimental errors. These data indicate that the USPIONs were not toxic for these tissue in the test conditions, and they did not affect cellular replication. Similar results were observed in the literature to other superparamagnetic iron oxide nanoparticles using the MTT method, where the USPIONs appear to be nontoxic towards tested cell lines.

For example, Tegafaw *et al*. demonstrated that the cell viability of DU145 and NCTC1469 cell lines treated with ultrasmall mixed Gd-Dy oxide nanoparticles did not differ significantly from untreated samples in concentrations up to 200 μmol L^{-1} [70]. This same behavior was observed by Zhang *et al*. since USPIONs did not affect rabbit hepatic

tumor cell viability tested concentrations range from 1 to 100 μg mL^{-1} in Fe, regardless of the duration of exposure from 4 to 24h [34]. Basirun *et al*. investigated the cytotoxicity of USPIONs in the WEHI164 (fibrosarcoma cells), treated with concentrations between 0.5 and 140 ppm for 24 hours, and showed no difference in cell viability when compared to the control [62].

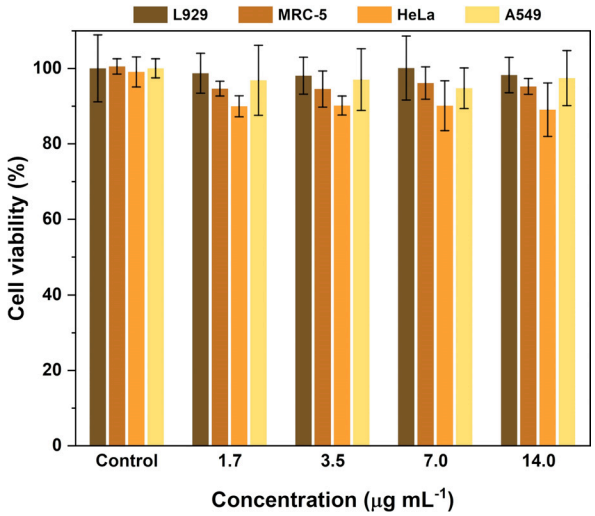

Fig. (6). Cell viability effect of USPIONs at different concentrations in four cell lines after 48 h treatment: L929 (connective fibroblasts from mice), MRC-5 lung nontumor cell line (ATCC® CCL-171), HeLa (human cervical carcinoma), and A549, lung adenocarcinoma (ATCC® CCL-185). (*A higher resolution / colour version of this figure is available in the electronic copy of the article*).

CONCLUSION

We successfully synthesized ultrasmall superparamagnetic iron oxide nanoparticles (USPIONs) with an average diameter of 3.4 nm in the magnetite phase using a micellar approach. The micelle solution was obtained using 1-octanol as the solvent and the Fe(III) dodecyl sulfate (IDS) surfactant, previously prepared from the substitution of the sodium ion in the sodium dodecyl sulfate. An IDS concentration 55% above its measured CMC generated reverse micelle with a hydrodynamic size of 3.8 nm, used as a template in the USPIONs' synthesis. The micelle solution was mixed with water resulting in a biphasic system to which sodium borohydride was added as a reducing agent. After the addition, a yellow precipitate immediately formed at the water/alcohol interface, quickly changing to black and transferring to the aqueous phase. Magnetic measurements at 5 K showed a major paramagnetic character with a weak ferromagnetic component. The low-temperature ferromagnetism has been assigned to interparticle coupling since the magnetic moment of the single-domain USPIONs remains blocked below 35 K (magnetic blocking temperature). The USPIONs coated with carboxymethyl dextran had an isoelectric point of 2.7 and an electrokinetic potential of -30 mV in the physiological pH range. Magnetic relaxation measurements showed relaxivity values of r_1 = 0.17 mM^{-1} s^{-1} and r_2 = 1.73 mM^{-1} s^{-1} with r_2/r_1 ratio of 10. Decreasing particle size decreases the magnetization of the magnetic core and its expected value for r_2. Simultaneously, r_1 is intensified because the surface area increases, allowing greater interaction with the protons of nearby water molecules. The data show the obtention of a system with high colloidal stability, non-cytotoxic against four tested cell lines, and potential application as T_1-T_2 dual-mode contrast agents.

LIST OF ABBREVIATIONS

D_{TEM}	=	Average Particle Size Determined by TEM Measurements
H_{hyp}	=	Hyperfine Filed Parameter (Mössbauer Spectroscopy)
T_B	=	Blocking Temperature
r_1	=	Longitudinal Relaxitivity Assigned to the T_1-Weighted Process
r_2	=	Transverse Relaxitivity Assigned to the T_2-Weighted Process
ν_{as}	=	Vibrational Asymmetric Stretching Mode
ν_s	=	Vibrational Symmetric Stretching Mode
AC	=	Absorbance of the Control Cells
APTS	=	3-Aminopropyltriethoxysilane
ATC	=	Absorbance of the Treated Cells
CMC	=	Critical Micelle Concentration
CMDex	=	Carboxymethyl Dextran
DLS	=	Dynamic Light Scattering
DMEM	=	Dulbelcco Modified Eagle Medium
EA	=	Elemental Analysis
EDS	=	Energy-Dispersive X-Ray Spectroscopy
FC	=	Field-Cooling Mode
FTIR	=	Fourier-Transform Infrared Spectroscopy
IDS	=	Iron(III) Dodecyl Sulfate
IEP	=	Isoelectric Point
JCPDS	=	Joint Committee on Powder Diffraction - International
MRI	=	Magnetic Resonance Imaging
MTT	=	3-(4,5-Dimethylthiazol-2-yl)-2,5-diphenyltetrazolium
PEG	=	Poly(Ethylene Glycol)
SD	=	Standard Deviation
SDS	=	Sodium Dodecyl Sulfate
SPIONs	=	Superparamagnetic Iron Oxide Nanoparticles
SQUID	=	Superconducting Quantum Interference Device
T_1	=	Longitudinal Magnetic Relaxation Time
T_2	=	Transverse Magnetic Relaxation Time
TE	=	Spin-Echo Time Parameter

TEM	=	Transmission Electron Microscopy
TGA-DTA	=	Thermogravimetric Analysis / Differential Thermogravimetric Analysis
TR	=	Long Time of Repetition Parameter
USPIONs	=	Ultrasmall Superparamagnetic Iron Oxide Nanoparticles
XRD	=	X-Ray Diffraction
ZFC	=	Zero-Field-Cooling Mode
Γ	=	Relative Area (Mössbauer Spectroscopy)
Δ	=	Quadrupolar Splitting (Mössbauer Spectroscopy)
δ	=	Isomer shift (Mössbauer Spectroscopy) or Vibrational Bending Mode
σ	=	Polydisperse Degree

AUTHORS' CONTRIBUTIONS

Watson Beck Jr., Simone J. S. Lopes, Daniel A. Moraes, Natalia M. Santos, and Maria Eduarda S. D. Lino1 conduct all experiments and characterizations performing the data analysis and contribute to data interpretation and discussion. Laudemir C. Varanda concepts the work idea and supervised all experiments and data analysis, interpretation, and discussion. The manuscript was written through the contributions of all authors. All authors have approved the final version of the manuscript.

ETHICS APPROVAL AND CONSENT TO PARTICIPATE

Not applicable.

HUMAN AND ANIMAL RIGHTS

Not applicable.

CONSENT FOR PUBLICATION

Not applicable.

AVAILABILITY OF DATA AND MATERIALS

The data that support the findings of this study are available from the corresponding author, [LCV], upon reasonable request.

FUNDING

This study was financed in part by the Coordenação de Aperfeiçoamento de Pessoal de Nível Superior - Brasil (CAPES, Finance Code 001) and FAPESP - Fundação de Amparo à Pesquisa do Estado de São Paulo, (Grant Numbers 2011/12210-4, 2013/01284-2, 2020/06501-5).

CONFLICT OF INTEREST

The authors declare that they have no known competing financial interests or personal relationships that could have appeared to influence the work reported in this paper.

ACKNOWLEDGEMENTS

The authors would like to thank the Brazilian funding agencies for their financial support (CAPES and FAPESP, see Funding information) and professors Dr. Fillipe V. Rocha (UFSCar) and Dr. Carlos EG Salmon (FFCLRP - USP) for their support in the measures of cytotoxicity and magnetic relaxation, respectively.

SUPPLEMENTARY MATERIAL

Supplementary materials are available on the publisher's website along with the published article.

REFERENCES

[1] Spanos A, Athanasiou K, Ioannou A, Fotopoulos V, Krasia-Christoforou T. Functionalized magnetic nanomaterials in agricultural applications. Nanomaterials (Basel) 2021; 11(11): 3106. http://dx.doi.org/10.3390/nano11113106 PMID: 34835870

[2] Kemp JA, Kwon YJ. Cancer nanotechnology: Current status and perspectives. Nano Converg 2021; 8(1): 34. http://dx.doi.org/10.1186/s40580-021-00282-7 PMID: 34727233

[3] Aslam H, Shukrullah S, Naz MY, Fatima H, Ullah S, Al-Sehemi AG. Multifunctional magnetic nanomedicine drug delivery and imaging-based diagnostic systems. Part Part Syst Charact 2021; 2100179(12): 2100179. http://dx.doi.org/10.1002/ppsc.202100179

[4] Li J, Xin M, Ma Z, Shi Y, Pan L. Nanomaterials and their applications on bio-inspired wearable electronics. Nanotechnology 2021; 32(47): 472002. http://dx.doi.org/10.1088/1361-6528/abe6c7 PMID: 33592596

[5] Kolahalam LA, Kasi Viswanath IV, Diwakar BS, Govindh B, Reddy V, Murthy YLN. Review on nanomaterials: Synthesis and applications. Mater Today Proc 2019; 18: 2182-90. http://dx.doi.org/10.1016/j.matpr.2019.07.371

[6] Varanda LC, Souza CGS, Moraes DA, *et al.* Size and shape-controlled nanomaterials based on modified polyol and thermal decomposition approaches. A brief review. An Acad Bras Cienc 2019; 91(4): e20181180. http://dx.doi.org/10.1590/0001-3765201920181180

[7] Laurent S, Forge D, Port M, *et al.* Magnetic iron oxide nanoparticles: Synthesis, stabilization, vectorization, physicochemical characterizations, and biological applications. Chem Rev 2008; 108(6): 2064-110. http://dx.doi.org/10.1021/cr068445e PMID: 18543879

[8] Roca AG, Costo R, Rebolledo AF, *et al.* Progress in the preparation of magnetic nanoparticles for applications in biomedicine. J Phys D Appl Phys 2009; 42(22): 224002. http://dx.doi.org/10.1088/0022-3727/42/22/224002

[9] Noqta OA, Aziz AA, Usman IA, Bououdina M. Recent Advances in Iron Oxide Nanoparticles (IONPs): Synthesis and surface modification for biomedical applications. J Supercond Nov Magn 2019; 32(4): 779-95. http://dx.doi.org/10.1007/s10948-018-4939-6

[10] Minaei SE, Khoei S, Khoee S, Vafashoar F, Mahabadi VP. *In vitro* anti-cancer efficacy of multi-functionalized magnetite nanoparticles combining alternating magnetic hyperthermia in glioblastoma cancer cells. Mater Sci Eng C 2019; 101: 575-87. http://dx.doi.org/10.1016/j.msec.2019.04.007 PMID: 31029351

[11] Castellanos-Rubio I, Rodrigo I, Olazagoitia-Garmendia A, *et al.* Highly reproducible hyperthermia response in water, agar, and cellular environment by discretely pegylated magnetite nanoparticles. ACS Appl Mater Interfaces 2020; 12(25): 27917-29. http://dx.doi.org/10.1021/acsami.0c03222 PMID: 32464047

[12] Oltolina F, Peigneux A, Colangelo D, *et al.* Biomimetic magnetite nanoparticles as targeted drug nanocarriers and mediators of hyperthermia in an experimental cancer model. Cancers (Basel) 2020; 12(9): E2564. http://dx.doi.org/10.3390/cancers12092564 PMID: 32916816

[13] Perecin CJ, Tirich BM, Nagamine LCCM, *et al.* Aqueous synthesis of magnetite nanoparticles for magnetic hyperthermia: Formation mechanism approach, high water-dispersity and stability. Colloids Surf A Physicochem Eng Asp 2021; 627: 127169. http://dx.doi.org/10.1016/j.colsurfa.2021.127169

[14] Berry CC. Progress in functionalization of magnetic nanoparticles for applications in biomedicine. J Phys D Appl Phys 2009; 42(22): 224003. http://dx.doi.org/10.1088/0022-3727/42/22/224003

[15] Gonçalves AI, Miranda MS, Rodrigues MT, Reis RL, Gomes ME. Magnetic responsive cell-based strategies for diagnostics and therapeutics. Biomed Mater 2018; 13(5): 054001. http://dx.doi.org/10.1088/1748-605X/aac78b PMID: 29794324

[16] Kheirkhah P, Denyer S, Bhimani AD, *et al.* Magnetic drug targeting: A novel treatment for intramedullary spinal cord tumors. Sci Rep 2018; 8(1): 11417. http://dx.doi.org/10.1038/s41598-018-29736-5 PMID: 30061692

[17] Hachani R, Birchall MA, Lowdell MW, *et al.* Assessing cell-nanoparticle interactions by high content imaging of biocompatible iron oxide nanoparticles as potential contrast agents for magnetic resonance imaging. Sci Rep 2017; 7(1): 7850. http://dx.doi.org/10.1038/s41598-017-08092-w PMID: 28798327

[18] Nosrati H, Salehiabar M, Fridoni M, *et al.* New insight about biocompatibility and biodegradability of iron oxide magnetic nanoparticles: Stereological and *in vivo* MRI monitor. Sci Rep 2019; 9(1): 7173. http://dx.doi.org/10.1038/s41598-019-43650-4 PMID: 31073222

[19] Lin G, Mu Q, Revia R, Stephen Z, Jeon M, Zhang M. A highly selective iron oxide-based imaging nanoparticle for long-term monitoring of drug-induced tumor cell apoptosis. Biomater Sci 2021; 9(2): 471-81. http://dx.doi.org/10.1039/D0BM00518E PMID: 32662460

[20] Branca M, Marciello M, Ciuculescu-Pradines D, *et al.* Towards MRI T_2 contrast agents of increased efficiency. J Magn Magn Mater 2015; 377: 348-53. http://doi.org/10.1016/j.jmmm.2014.10.086

[21] El-Gendy HA, Harstad SM, Vijayaragavan V, *et al.* Ferromagnetic Gd_5Si_4 nanoparticles as T_2 contrast agents for magnetic resonance imaging. IEEE Magn Lett 2017; 8: 1-4. http://dx.doi.org/10.1109/LMAG.2017.2728503

[22] Ramalho J, Semelka RC, Ramalho M, Nunes RH, AlObaidy M, Castillo M. Gadolinium-based contrast agent accumulation and toxicity: An update. AJNR Am J Neuroradiol 2016; 37(7): 1192-8. http://dx.doi.org/10.3174/ajnr.A4615 PMID: 26659341

[23] Neves H R, Bini R A, Barbosa J H O, Salmon C E G, Varanda L C. Dextran-coated antiferromagnetic mno nanoparticles for a T-1-MRI contrast agent with high colloidal stability. Part Part Syst Char 2016; 33(3): 167-76. http://dx.doi.org/10.1002/ppsc.201500251

[24] Wang G, Gao W, Zhang X, Mei X. Au nanocage functionalized with ultra-small Fe_3O_4 nanoparticles for targeting T_1-T_2Dual MRI and CT imaging of tumor. Sci Rep 2016; 6(1): 28258. http://dx.doi.org/10.1038/srep28258 PMID: 27312564

[25] Arami H, Khandhar AP, Tomitaka A, *et al. In vivo* multimodal magnetic particle imaging (MPI) with tailored magneto/optical contrast agents. Biomaterials 2015; 52: 251-61. http://dx.doi.org/10.1016/j.biomaterials.2015.02.040 PMID: 25818431

[26] Alipour A, Soran-Erdem Z, Utkur M, *et al.* A new class of cubic SPIONs as a dual-mode T_1 and T_2 contrast agent for MRI. Magn Reson Imaging 2018; 49: 16-24. http://dx.doi.org/10.1016/j.mri.2017.09.013 PMID: 28958878

[27] Chen C, Ge J X, Gao Y, *et al.* Ultrasmall superparamagnetic iron oxide nanoparticles: A next generation contrast agent for magnetic resonance imaging. WIREs Nanomed Nanobiotechnol 2021; e1740. http://dx.doi.org/10.1002/wnan.1740

[28] Kim BH, Lee N, Kim H, *et al.* Large-scale synthesis of uniform and extremely small-sized iron oxide nanoparticles for high-resolution T_1 magnetic resonance imaging contrast agents. J Am Chem Soc 2011; 133(32): 12624-31. http://dx.doi.org/10.1021/ja203340u PMID: 21744804

[29] Liu D, Li J, Wang C, *et al.* Ultrasmall Fe@Fe_3O_4 nanoparticles as T_1-T_2 dual-mode MRI contrast agents for targeted tumor imaging. Nanomedicine 2021; 32: 102335. http://dx.doi.org/10.1016/j.nano.2020.102335 PMID: 33220508

[30] Lee N, Yoo D, Ling D, Cho MH, Hyeon T, Cheon J. Iron oxide based nanoparticles for multimodal imaging and magnetoresponsive therapy. Chem Rev 2015; 115(19): 10637-89. http://dx.doi.org/10.1021/acs.chemrev.5b00112 PMID: 26250431

[31] Johnson J Jr, Pajarillo E, Karki P, *et al.* Valproic acid attenuates manganese-induced reduction in expression of GLT-1 and GLAST with concomitant changes in murine dopaminergic neurotoxicity. Neurotoxicology 2018; 67: 112-20. http://dx.doi.org/10.1016/j.neuro.2018.05.001 PMID: 29778792

[32] Pajarillo E, Johnson J Jr, Kim J, *et al.* 17β-estradiol and tamoxifen protect mice from manganese-induced dopaminergic neurotoxicity. Neurotoxicology 2018; 65: 280-8. http://dx.doi.org/10.1016/j.neuro.2017.11.008 PMID: 29183790

[33] Fernandez-Barahona I, Munoz-Hernando M, Ruiz-Cabello J, Herranz F, Pellico J. Iron oxide nanoparticles: An alternative for positive contrast in magnetic resonance imaging. Inorganics (Basel) 2020; 8(4): 28. http://dx.doi.org/10.3390/inorganics8040028

[34] Bai C, Hu PC, Liu NL, *et al.* Synthesis of ultrasmall Fe_3O_4 nanoparticles as T_1-T_2 dual-modal magnetic resonance imaging contrast agents in rabbit hepatic tumors. ACS Appl Nano Mater 2020; 3(4): 3585-95. http://dx.doi.org/10.1021/acsanm.0c00306

[35] Wei H, Bruns OT, Kaul MG, *et al.* Exceedingly small iron oxide nanoparticles as positive MRI contrast agents. Proc Natl Acad Sci USA 2017; 114(9): 2325-30. http://dx.doi.org/10.1073/pnas.1620145114 PMID: 28193901

[36] Bai C, Jia ZY, Song LN, *et al.* Time-dependent T_1-T_2 switchable magnetic resonance imaging realized by c(RGDyK) modified ultrasmall Fe_3O_4 nanoprobes. Adv Funct Mater 2018; 28(32): 1802281. http://dx.doi.org/10.1002/adfm.201802281

[37] Ni D, Bu W, Ehlerding EB, Cai W, Shi J. Engineering of inorganic nanoparticles as magnetic resonance imaging contrast agents. Chem Soc Rev 2017; 46(23): 7438-68. http://dx.doi.org/10.1039/C7CS00316A PMID: 29071327

[38] Jeon M, Halbert MV, Stephen ZR, Zhang M. Iron oxide nanoparticles as T_1 contrast agents for magnetic resonance imaging: Fundamentals, challenges, applications, and prospectives. Adv Mater 2021; 33(23): e1906539. http://dx.doi.org/10.1002/adma.201906539 PMID: 32495404

[39] Shin TH, Choi Y, Kim S, Cheon J. Recent advances in magnetic nanoparticle-based multi-modal imaging. Chem Soc Rev 2015; 44(14): 4501-16. http://dx.doi.org/10.1039/C4CS00345D PMID: 25652670

[40] Zhou Z, Yang L, Gao J, Chen X. Structure-relaxivity relationships of magnetic nanoparticles for magnetic resonance imaging. Adv Mater 2019; 31(8): e1804567. http://dx.doi.org/10.1002/adma.201804567 PMID: 30600553

[41] Varanda LC, Souza CGSd, Perecin CJ, *et al.* Inorganic and organic-inorganic composite nanoparticles with potential biomedical applications: Synthesis challenges for enhanced performance.Materials for Biomedical Engineering. Amsterdam: Elsevier 2019; pp. 47-99. http://dx.doi.org/10.1016/B978-0-12-818431-8.00004-0

[42] Marciello M, Connord V, Veintemillas-Verdaguer S, *et al.* Large scale production of biocompatible magnetite nanocrystals with high saturation magnetization values through green aqueous synthesis. J Mater Chem B Mater Biol Med 2013; 1(43): 5995-6004. http://dx.doi.org/10.1039/c3tb20949k PMID: 32261067

[43] Kokubo T, Takadama H. How useful is SBF in predicting *in vivo* bone bioactivity? Biomaterials 2006; 27(15): 2907-15. http://dx.doi.org/10.1016/j.biomaterials.2006.01.017 PMID: 16448693

[44] Mosmann T. Rapid colorimetric assay for cellular growth and survival: Application to proliferation and cytotoxicity assays. J Immunol Methods 1983; 65(1-2): 55-63.
http://dx.doi.org/10.1016/0022-1759(83)90303-4 PMID: 6606682

[45] Mukerjee P, Mysels K, Kapauan P. Counterion specificity in the formation of ionic micelles - size. J Phys Chem 1967; 71(13): 4166-75.
http://dx.doi.org/10.1021/j100872a702

[46] Sanchez-Fernandez A, Hammond O S, Edler K J, *et al.* Counterion binding alters surfactant self-assembly in deep eutectic solvents. 2018; 20(20): 13952-61.
http://dx.doi.org/10.1039/C8CP01008K

[47] Fioretto D, Freda M, Onori G, Santucci A. Effect of counterion substitution on AOT-based micellar systems: dielectric study of Cu(AOT)2 reverse micelles in CCl4. 1999; 103(39): 8216-20.
http://dx.doi.org/10.1021/jp9918048

[48] Cushing BL, Kolesnichenko VL, O'Connor CJ. Recent advances in the liquid-phase syntheses of inorganic nanoparticles. Chem Rev 2004; 104(9): 3893-946.
http://dx.doi.org/10.1021/cr030027b PMID: 15352782

[49] Veisi H, Maleki B, Eshbala FH, *et al. In situ* generation of Iron(III) dodecyl sulfate as Lewis acid-surfactant catalyst for synthesis of bis-indolyl, tris-indolyl, Di(bis-indolyl), Tri(bis-indolyl), tetra(bis-indolyl)methanes and 3-alkylated indole compounds in water. RSC Advances 2014; 4(58): 30683-8.
http://dx.doi.org/10.1039/C4RA03194F

[50] Mahmoodi NO, Jalalifard Z, Fathanbari GP. Green synthesis of bis-coumarin derivatives using $Fe(SD)_3$ as a catalyst and investigation of their biological activities. J Chin Chem Soc (Taipei) 2020; 67(1): 172-82.
http://dx.doi.org/10.1002/jccs.201800444

[51] Nakamoto K. Infrared and raman spectra of inorganic and coordination compounds, part a: theory and applications in inorganic chemistry. Wiley 2009.

[52] Pereira RFP, Valente AJM, Burrows HD, de Zea Bermudez V, Carvalho RA, Castro RAE. Structural characterization of solid trivalent metal dodecyl sulfates: From aqueous solution to lamellar superstructures. RSC Adv 2013; 3(5): 1420-33.
http://dx.doi.org/10.1039/C2RA21906A

[53] Machida M, Kawamura K, Kawano T, Zhang D, Ikeue K. Layered Pr-dodecyl sulfate mesophases as precursors of $Pr_2O_2SO_4$ having a large oxygen-storage capacity. J Mater Chem 2006; 16(30): 3084-90.
http://dx.doi.org/10.1039/b605518d

[54] Bai B, Hankins N P, Hey M J, Kingman S W. *In situ* mechanistic study of SDS adsorption on hematite for optimized froth flotation. Ind Eng Chem Res 2004; 43(17): 5326-38.
http://dx.doi.org/10.1021/ie034307t

[55] Hadjiivanov KI. Identification of neutral and charged N_x O_y surface species by IR spectroscopy. Catal Rev, Sci Eng 2000; 42(1-2): 71-144.
http://dx.doi.org/10.1081/CR-100100260

[56] Mihaylov MY, Ivanova EZ, Vayssilov GN, Hadjiivanov KI. Revisiting ceria-NO^x interaction: FTIR studies. 2020; 357: 613-20.
http://dx.doi.org/10.1016/j.cattod.2019.05.014

[57] Darbandi M, Stromberg F, Landers J, *et al.* Nanoscale size effect on surface spin canting in iron oxide nanoparticles synthesized by the microemulsion method. J Phys D Appl Phys 2012; 45(19): 195001.
http://dx.doi.org/10.1088/0022-3727/45/19/195001

[58] Wongwailikhit K, Horwongsakul S. The preparation of iron (III) oxide nanoparticles using W/O microemulsion. Mater Lett 2011; 65(17-18): 2820-2.
http://dx.doi.org/10.1016/j.matlet.2011.05.063

[59] Pileni MP. Nanosized particles made in colloidal assemblies. Langmuir 1997; 13(13): 3266-76.
http://dx.doi.org/10.1021/la960319q

[60] Cornell RM, Schwertmann U. The Iron oxides: structure, properties, reactions, occurrences and uses. 2nd ed. Weinheim: Wiley-VCH 2006.

[61] Daou TJ, Pourroy G, Begin-Colin S, *et al.* Hydrothermal synthesis of monodisperse magnetite nanoparticles. Chem Mater 2006; 18(18): 4399-404.
http://dx.doi.org/10.1021/cm060805r

[62] Rasouli E, Basirun WJ, Rezayi M, *et al.* Ultrasmall superparamagnetic Fe_3O_4 nanoparticles: Honey-based green and facile synthesis and *in vitro* viability assay. Int J Nanomedicine 2018; 13: 6903-11.
http://dx.doi.org/10.2147/IJN.S158083 PMID: 30498350

[63] Goya GF, Berquo TS, Fonseca FC, Morales MP. Static and dynamic magnetic properties of spherical magnetite nanoparticles. J Appl Phys 2003; 94(5): 3520-8.
http://dx.doi.org/10.1063/1.1599959

[64] Cullity BD, Graham CD. Introduction to magnetic materials. 2nd ed. New Jersey, USA: IEEE Press 2008; p. 832.
http://dx.doi.org/10.1002/9780470386323

[65] Kim BH, Hackett MJ, Park J, Hyeon T. Synthesis, characterization, and application of ultrasmall nanoparticles. Chem Mater 2014; 26(1): 59-71.
http://dx.doi.org/10.1021/cm402225z

[66] Glisic S, Nikolic G, Cakic M, Trutic N. Spectroscopic study of copper(II) complexes with carboxymethyl dextran and dextran sulfate. Russ J Phys Chem A Focus Chem 2015; 89(7): 1254-62.
http://dx.doi.org/10.1134/S0036024415070122

[67] Herrera AP, Barrera C, Rinaldi C. Synthesis and functionalization of magnetite nanoparticles with aminopropylsilane and carboxymethyldextran. J Mater Chem 2008; 18(31): 3650-4.
http://dx.doi.org/10.1039/b805256e

[68] Hajesmaeelzadeh F, Shanehsazzadeh S, Grüttner C, Daha FJ, Oghabian MA. Effect of coating thickness of iron oxide nanoparticles on their relaxivity in the MRI. Iran J Basic Med Sci 2016; 19(2): 166-71.
PMID: 27081461

[69] Schladt TD, Koll K, Prufer S, *et al.* Multifunctional superparamagnetic $MnO@SiO_2$ core/shell nanoparticles and their application for optical and magnetic resonance imaging. J Mater Chem 2012; 22(18): 9253-62.
http://dx.doi.org/10.1039/c2jm15320c

[70] Tegafaw T, Xu W, Ahmad MW, *et al.* Dual-mode T1 and T2 magnetic resonance imaging contrast agent based on ultrasmall mixed gadolinium-dysprosium oxide nanoparticles: Synthesis, characterization, and *in vivo* application. Nanotechnology 2015; 26(36): 365102.
http://dx.doi.org/10.1088/0957-4484/26/36/365102
PMID: 26291827